A R C H I V E S O F M E T A L L U R G Y A N D M A T E R I A L S
Volume 57 2012 Issue 4
DOI: 10.2478/v10172-012-0137-x

A. KULAWIK*

MODELING OF THERMOMECHANICAL PHENOMENA OF WELDING PROCESS OF STEEL PIPE

MODELOWANIE ZJAWISK TERMOMECHANICZNYCH PROCESU SPAWANIA RURY STALOWEJ

In this paper an analysis of phenomena of laser welding of steel thin-walled element is presented. Coupled mathematical and numerical models of thermal phenomena, mechanical and phase transitions in solid and liquid state are proposed. To the modeling of phase transformation in the solid state the macroscopic model based on the analysis of the CTP diagrams are used. In the simulation of thermal phenomena the solution of heat transport equations with melting and solidification model is applied. Mechanical phenomena using the stress model for a elastic-plastic range and the isotropic strengthening of material are simulated. In order to solve analyzed problem the software using the finite element method (3D problem)has been developed. The influence of the individual elements of the model on the stress field and the plastic deformation field of welded steel element is determined. A comparative analysis of the results of numerical calculations for the case: the dependence of material properties on the temperature, the inclusion of phase transformation in the solid state, the dependence of the yield strength on the phase composition of the material are made.

Keywords: numerical model, welding, phase transformations, stresses

W prezentowanej pracy przeprowadzono analizę zjawisk spawania laserowego stalowego elementu cienkościennego. Zaproponowano sprzężone modele matematyczne oraz numeryczne zjawisk cieplnych, mechanicznych oraz przemian fazowych w stanie stałym i ciekłym. Do modelowania przemian fazowych w stanie stałym wykorzystano makroskopowy model zbudowany z wykorzystaniem analizy wykresów CTP. Do symulacji zjawisk termicznych zastosowano rozwiązanie równania przewodzenia ciepła z modelem topienia i krzepnięcia w ujęciu pojemnościowym. Zjawiska mechaniczne symulowano z wykorzystaniem modelu naprężeń dla zakresu sprężysto-plastycznego i wzmocnieniem izotropowym materiału. Do rozwiązania zadań stworzono oprogramowanie wykorzystujące metodę elementów skończonych (zadania 3D). Określono wpływ poszczególnych elementów modelu na uzyskane pola naprężeń oraz pola deformacji plastycznych spawanego elementu stalowego. Przeprowadzono analizę porównawczą otrzymanych wyników obliczeń dla przypadków z elementami modelu takimi jak zmienność parametrów materiału od temperatury, uwzględnienie przemian fazowych w stanie stałym, zależność granicy plastyczności od składu fazowego materiału.

1. Introduction

Welding as a process of joining of material is often used in modern industry. Depending on the type of heat source different welding methods are distinguished. Independently on the selected type of welding method we deal with a similar range of phenomena. First of all the phenomenon of the thermal, the phase transformations in the solid and the liquid state, the mechanical phenomena, sometimes the diffusion phenomena occurring especially when the joint of materials is made by additional material made by material different than base material (BM) should be mentioned. The quality of the welded joint is dependent on many factors. There are many different types of weld defects, and all should be eliminated. Even if the welded joint meets all the quality requirements and it is imperfection free (no shape imperfections and no internal imperfections such as porosity or nonmetallic inclusions, cracks, etc.) it may not be acceptable because of the excessive welding stress. The cracks released by welding stress may also occur during the exploitation of the welded part. Minimization of residual stresses depends on the selection of the various parameters. It is often impossible to estimate without additional expensive research test. The test of welded joint - X-rays, is often insufficient to define the quality of the welded joint. The information about the quality of the welded joint can be achieved also by the series of the very costly experimental tests.

* INSTITUTE OF COMPUTER AND INFORMATION SCIENCES, CZESTOCHOWA UNIVERSITY OF TECHNOLOGY, 42-200 CZĘSTOCHOWA, 73 DĄBROWSKI STR., POLAND

Nowadays, to estimate the state of stress in welded steel elements the numerical methods are used. Computer simulations allow to reduce the cost of development and production welded parts.

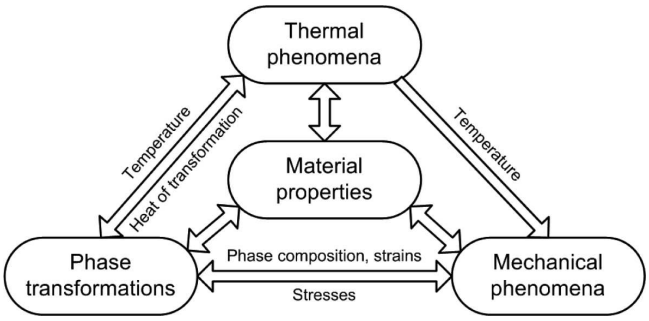

Fig. 1. The relationship diagram of the numerical model of welding process

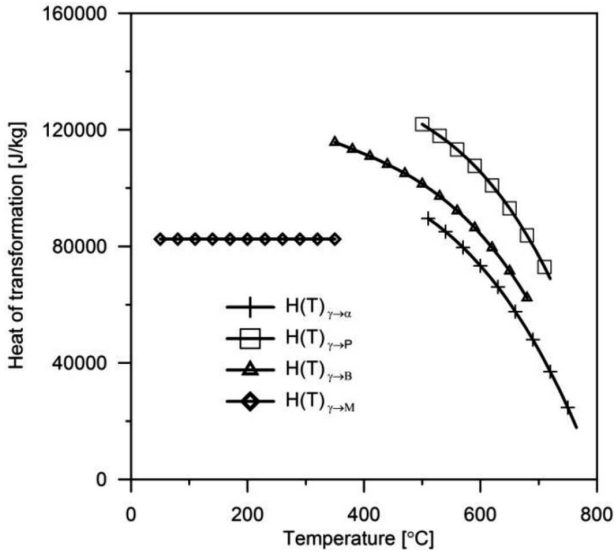

Fig. 2. The latent heat of transformation for phase transformations in solid state (medium carbon steel)

2. Temperature fields

In presented model of welding, determination the changes of temperature is very important. To calculate of the temperature field, the partial differential equation description for unsteady heat transfer is used:

$$\nabla \cdot (\lambda \nabla T) - c\rho \frac{\partial T}{\partial t} + q_V = 0 \tag{1}$$

where: $\lambda = \lambda(T)$ is the thermal conductivity coefficient, $c = c(T)$ is the thermal capacity, ρ is the density and $q_V = q_V(x_\alpha, t)$ is the volumetric heat source coming from latent heat of transformations, x_α is the vector location of considered point.

Phase transformations in the solid state generate considerable quantity of heat. Particularly intensive in transformation of austenite to pearlite. In the presented model the latent heat of these transformation as volumetric heat source in heat transfer equation is introduced.

$$\dot{q}_V = \sum_i H_i \frac{\Delta \eta_i}{\Delta t} \rho \tag{2}$$

where: $H_i[J/kg]$ is the heat of "i" transformation, $\Delta\eta_i$ is the volumetric increment of phase "i".

Changes of temperature, which are caused by latent heat of phase transformations, are most visible during cooling process of high carbon steel [1,2]. In presented paper the results of analysis of Fe-C-Mn system and constant value of enthalpy for austenite-martensite transformation are used [1,3]. Latent heat of transformation has influence especially on temperature changes and kinetics of phase transformations in the volumetric hardening, whereas it is insignificant in transformations during the surface hardening (Fig. 2).

In the model of welding the changes in the temperature fields caused by solidification and melting of the material should be included. In the presented model these phenomena by changing the effective heat capacity are considered.

The effective heat capacity of the material in the melting process is determined by the function describing the enthalpy depending on the temperature [4,5]

$$C_{ef} = \frac{dH}{dT} \tag{3}$$

where $H = H(T)$ is a known function of enthalpy.

Therefore [4,5]

$$C_{ef} = \rho(T)\, c(T) - \rho_S L \left. \frac{\partial f_S(T)}{\partial T} \right|_{T_S}^{T_L} \tag{4}$$

where L[J/(kgK)] is a latent heat of transformation of the liquid phase – solid phase.

The share of the solid phase is determined by the lever rule.

$$f_S = f_S(T) = \frac{T_L - T}{T_L - T_S}, \quad T \in [T_L, T_S] \tag{5}$$

where T_L is the temperature of liquidus line, T_S temperature of solidus line.

In the presented model the laser heating is modeled. In the numerical model of heating the hybrid model of source is also included. This source is a combination of superficial and internal sources.

The superficial source (Fig. 3.) is described by the following formula (Neumann boundary condition) [6]:

$$q_N(x,z) = \frac{F}{2\pi R^2} \exp\left(-\frac{(x-x_0)^2 + (z-z_0)^2}{2R^2}\right) \tag{6}$$

where F [W] is the power of superficial source, $\sqrt{2}R$ [m] – radius of the source, x_0 and z_0 [m] – coordinates of the centre of source.

Inside the heated area, under the surface of superficial boundary condition, the volumetric heat source is taken into account

$$q_V(x,z) = \frac{Q}{2\pi R^2 h} \exp\left(-\frac{(x-x_0)^2 + (z-z_0)^2}{2R^2}\right) \tag{7}$$

where Q [W] is the power of internal source, h [m] – depth of volumetric source.

Distribution of values of the volumetric heat source is constant on the wall thickness of the steel pipe (Fig. 4.).

The heat transport equation with completed boundary and initial conditions in finite element method of Bubnov-Galerkin formulation is solved. System of equation after aggregation is in the form [7,8]

where: s is the next step of time, $\gamma(\gamma \in [0,1])$ a parameter dependent on the type of time integration scheme, K_{ij} is heat conductivity matrix, M_{ij} heat capacity matrix, B_{ij} is right hand side vector, Q_{ij} volumetric heat source matrix.

These matrix by following integrals are determined

$$\begin{aligned} K_{ij}^e &= \rho c \int_{\Omega^e} \left(\lambda w_{i,\alpha} \Phi_{j,\alpha}\right) d\Omega, \quad M_{ij} = \frac{\rho c}{\Delta t} \int_{\Omega^e} w_i \Phi_j d\Omega, \\ B_{ij}^e &= \int_{\Gamma_Q^e} \Phi_j w_i d\Gamma + \int_{\Gamma_N^e} \alpha^\infty w_i \Phi_j d\Gamma = \left(B_{ij}^Q\right)^e + \left(B_{ij}^{NR}\right)^e, \\ Q_{ij}^e &= \int_{\Omega^e} w_i \Phi_j d\Omega \end{aligned} \tag{9}$$

where w_i are the weighting functions, Φ_i – shape functions.

$$\begin{aligned} &\left(\gamma\left(K_{ij} + B_{ij}^{NR}\right) + M_{ij}\right) T_j^{(s+1)} = \left(M_{ij} - (1-\gamma)\left(K_{ij} + B_{ij}^{NR}\right)\right) T_j^{(s)} + \\ &+\gamma\left(B_{ij}^{NR} T_j^{\infty(s+1)} - B_{ij}^Q q_j^{*(s+1)} + Q_{ij} q_j^{V(s+1)}\right) + (1-\gamma)\left(B_{ij}^{NR} T_j^{\infty(s)} - B_{ij}^Q q_j^{*(s)} + Q_{ij} q_j^{V(s)}\right) \end{aligned} \tag{8}$$

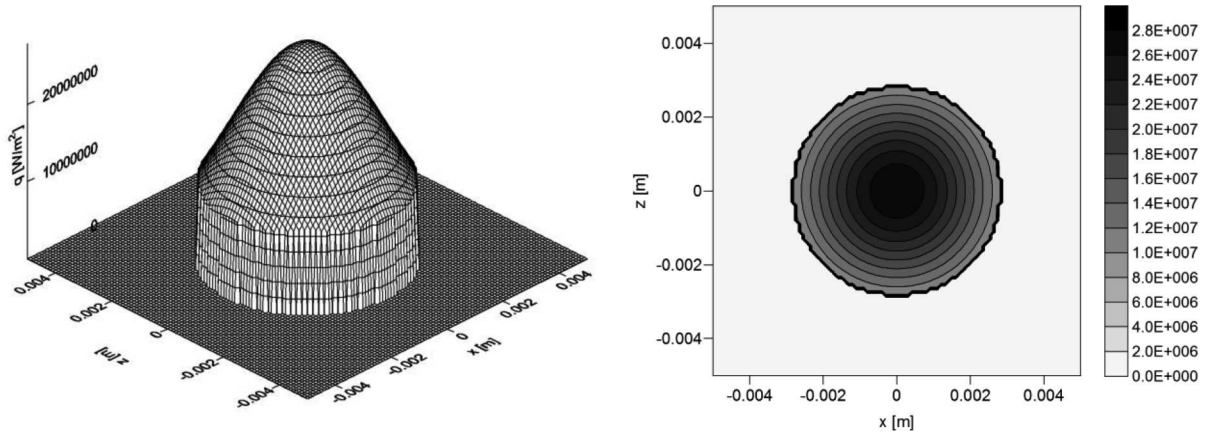

Fig. 3. Graphic interpretation of the superficial heat source

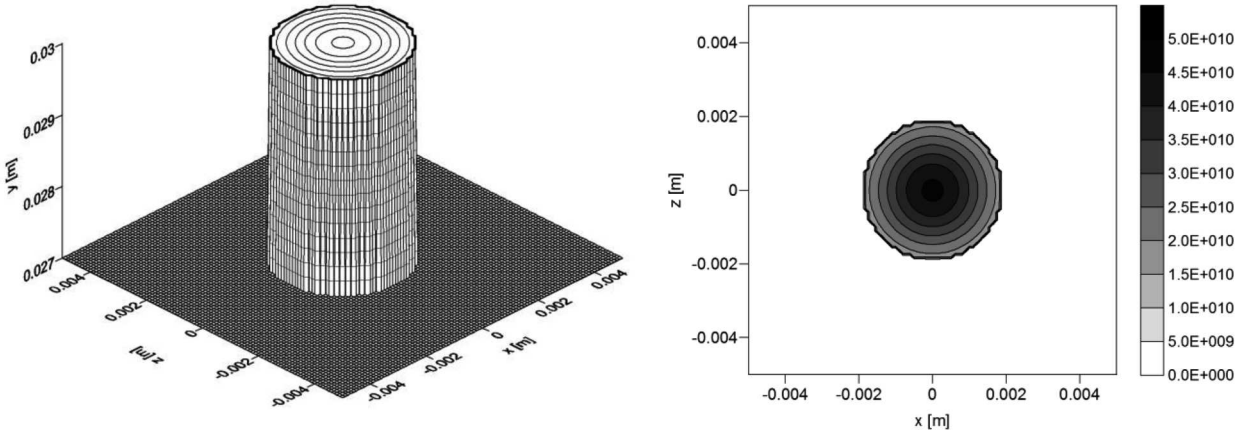

Fig. 4. Graphic interpretation of the volumetric heat source

Because the equation (1) in the Lagrangian coordinates is solved, the boundary condition of the heat source must be updated at each time step. Changes in the boundary conditions of modeled steel pipe, during cooling by radiation and convection are also included. Cooling conditions at the outer and inner boundary of pipe have been taken into account. The solution of the problem for the half of the steel element is calculated (due to symmetry of the considered geometry). On the plane of symmetry the front boundary (Γ_F) is located.

3. Model of phase kinetics during heating

In the process of heating occurs the transformation of phases to austenite. The start and finish of phase transformation strongly depend on heating rate or time of holding. The CHT diagram of steel include the dynamical A_{c1} and A_{c3} curves and the homogenization curve [9,10]. These curves presents decompositions of phases, which are formed during heating process. Above the curve of homogenization non-advisable growth grains of austenite can be observed.

In every step the fraction of new phase for high rate of heating is calculated on the basis of modified Koistinen-Marburger equation [7,11]:

$$\tilde{\eta}_\gamma(T,t) = 1 - \exp\left(-k_\gamma\left(T_{s\gamma} - T\right)\right),\ k_\gamma = \frac{4{,}60517}{\mathrm{T_{s\gamma}} - T_{f\gamma}} \tag{10}$$

where: $\mathrm{T}_{s\gamma}$ is start temperature of austenite formation, $\mathrm{T}_{f\gamma}$ is estimated finish temperature of transformation depend on rate of heating.

4. Phase transformations of cooling

The modeling of the cooling process should take into consideration the phase transformations in the solid state. These transformations influence on the temperature field through the heat of transformation and also have a significant impact on the field of stresses. To modeling of these phase transformations the macroscopic model is used. This model on an analysis of CCT diagrams is based. [10].

The volume fractions $\eta_{(.)}(T,t)$ growth during cooling process are calculated by the Avrami equations [5,10,12,13].

$$\eta_{(i)}(T,t) = \min\left\{\eta_{(i\%)}, \tilde{\eta}_\gamma - \sum_{j\neq i}\eta_j\right\}\cdot\left(1 - \exp\left(-b(T)\,t^{n(T)}\right)\right) \tag{11}$$

where: $\tilde{\eta}_\gamma$ is a volume fraction of forming austenite, η_j is volume fraction of phase formed during cooling process, $\eta_{(i\%)}$ is final fraction of "i" – phase estimation of basis on CCT diagrams considered steel. The functions $b(T)$ and $n(T)$ depending on temperature as well as on the start (t_s) and finish (t_f) times of transformation is described by formulas:

$$n(T) = 6{,}12733/\ln\left(\frac{t_f(T)}{t_s(T)}\right),\qquad b(T) = \frac{0{,}01005}{\mathrm{t_s}^{n(T)}} \tag{12}$$

The results obtained from Avrami equation strongly depend on the assumed CCT diagram analysis. The function determined by the Avrami covers the whole range transformation and must be appropriately modified for the analysis of individual transformation. Is assumes that the function is defined in segments depending on the location of the transformation in the CCT diagram. Coefficients occurring in these functions are obtained from CCT diagram. In paper the model, which determinate the kinetics of individual phases with the use of spline functions is applied [7,13].

The phase transformation during the high-rate cooling (transformation austenite to martensite) is determined by Koistinen-Marburger equation (for T<Ms) [7,9,11]:

$$\eta_M(T,t) = \left(\tilde{\eta}_\gamma - \sum_{i\neq M}\eta_i\right)\left(1 - \exp\left(-k\left(M_S - T + A_M\sigma_{eff} + B_M(\sigma_{ii})/3\right)\right)\right),\quad k = 0.01537 \tag{13}$$

where: $\sigma_{eff} = \sqrt{3/2\,(\sigma^D\cdot\sigma^D)}$ – effective stress, σ^D – deviatoric stresses, A_M and B_M – material coefficients [14].

The increase of isotropic strain resulted from the temperature and phase transformation ($d\varepsilon^{Tph} = d\varepsilon^T + d\varepsilon^{ph}$) during heating and cooling is described by formula [7,13]:

$$d\varepsilon^T = \sum_i \alpha_i(T)\,\eta_i dT,\quad d\varepsilon^{ph} = \sum_i \varepsilon_i^{ph}(T)\,d\eta_i \tag{14}$$

where: α_i is a thermal expansion coefficients for "i" phase, $\varepsilon_i^{ph} = \delta V_i/(3V)$ is a strain expansion coefficients for "i" transformation. Experimental research and numerical simulations – dilatometric curves, assign these values (thermal and structural expansion coefficients) [7].

During the welding process the tempering phenomena has also occurred. In the presented model the transformation of martensite to sorbite is calculated by the modified Avrami equation. The temperature of start and finish of transformation are determined by the equations [15]:

$$T_S(V_H) = A_S B_S^{V_H}(V_H)^{C_S},\ T_F(V_H) = \frac{1}{A_F + B_F V_H^{C_F}} \tag{15}$$

where: V_H [°C/s] – the heating rate, A_S =306.1645, B_S =1.0007, C_S =0.0251, A_F =0.0026, B_F =-0.00028, C_F =0.1568 (coefficients for medium carbon steel)[15].

5. Model of mechanical phenomena

During the welding process the strong changes of temperature is occurred. This changes and phase transformations in the steel elements cause a sudden changes in stress fields. This changes are the result of different types of strains and changes of material properties (yield point and Young's modulus). In the presented model, except elastic ($\varepsilon^{\mathbf{e}}$), thermal ($\varepsilon^{\mathbf{T}}$), structural ($\varepsilon^{\mathbf{ph}}$) and plastic ($\varepsilon^{\mathbf{pl}}$) strains, the transformations plasticity ($\varepsilon^{\mathbf{tp}}$) and changes of material properties ($\Delta\mathbf{D}$) are taken into accounts as well ($\varepsilon = \varepsilon^{\mathbf{e}}+\varepsilon^{\mathbf{T}}+\varepsilon^{\mathbf{ph}}+\varepsilon^{\mathbf{pl}}+\varepsilon^{\mathbf{tp}}$) [7,9,13,16].

The constitutive relations are assumed in the form:

$$\Delta\boldsymbol{\sigma} = \mathbf{D} \circ \Delta\boldsymbol{\varepsilon}^{\mathbf{e}} + \Delta\mathbf{D} \circ \boldsymbol{\varepsilon}^{\mathbf{e}} \tag{16}$$

where: $\boldsymbol{\sigma}$ is tensor of stress, $\mathbf{D}$ is tensor of material constants.

In presented model (Fig. 5.) increment of plastic strain is determined by nonisothermic plastic flow law:

$$\dot{\boldsymbol{\varepsilon}}^{\mathbf{pl}} = \dot{\lambda}\frac{3\boldsymbol{\sigma}^{\mathbf{D}}}{2\bar{\sigma}} \tag{17}$$

in which scalar plastic multiplier is calculated by Newton-Raphson method (isotropic hardening) [16].

The actual level of effective stress ($\bar{\sigma}$) is depended on temperature and composition of phase:

$$\bar{\sigma}\left(T, \sum_i \eta_i, \varepsilon^{pl}_{eff}\right) = \bar{\sigma}_0\left(T, \sum_i \eta_i\right) + \kappa\left(T\right)\varepsilon^{pl}_{eff} \tag{18}$$

where: $\bar{\sigma}_0$ is the yield point, ε^{pl}_{eff} is the effective plastic strain, κ is the hardening modulus dependent on Young's and tangential modulus.

The yield point depends on volume fractions of phase, is completed by nonlinear influence of hard phase (martensite) [9]:

$$\bar{\sigma}_0\left(T, \sum_i \eta_i\right) = \sum_{i\neq M} \eta_i \bar{\sigma}_i\left(T\right) + f\left(\eta_M\right)\bar{\sigma}_M\left(T\right) \tag{19}$$

where: $\bar{\sigma}_i$, $\bar{\sigma}_M$ are the yield points of particular phases [17], $f = f\left(\eta_M\right)$ is the function of influence of martensite.

Transformations induced plasticity ε^{tp} are non-reversible changes observed during phase transformations occur under loading (in state of stress). In the models based on Greenwood-Johnson mechanism transformations induced plasticity is described by the following formula [7,9,18]:

$$\dot{\boldsymbol{\varepsilon}}^{tp} = \sum_i \frac{5}{4}\frac{\delta V_i}{V} K_i F\left(\eta_i\right)\frac{\boldsymbol{\sigma}^D}{\bar{\sigma}}\dot{\eta}_i \tag{20}$$

where: $F\left(\eta_i\right) = -\ln\left(\eta_i\right)$ (Leblond [9,17]) is a function which determine kinetics of transformation plasticity.

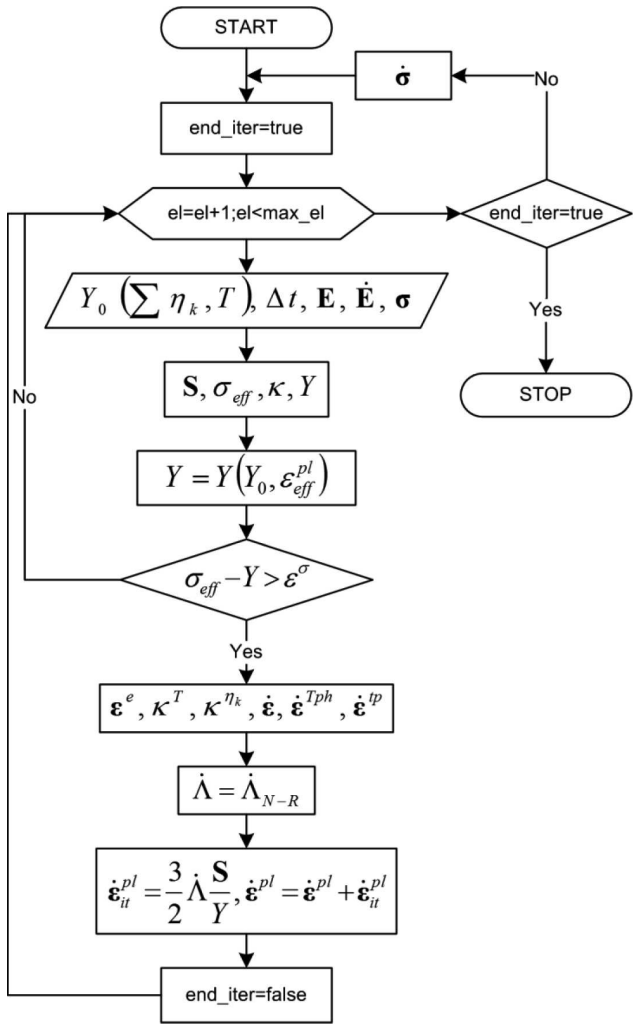

Fig. 5. The flow diagram of the numerical model of determination of plastic strains

6. Examples of calculation

The geometry of the welding pipe is presented in Fig. 6. The effects of the phase transformations, dependence of the yield point on the temperature and composition of phase on distribution of the temporary stresses were investigated. The comparative analysis of results of calculations for the model taking and not taking into account particular element of numerical model has been carried out. In the paper calculations for the 3-dimmensional model of pipe have been presented.

The dimensions of the medium carbon steel elements are following: outer radius r_o =0.03 m, the pipe wall thickness is h =0.003 m, the length of analyzed pipe (distance from the weld to the handle) is 0.05 m. Results of numerical calculations show differences between assumed models of welding. In the first model (example 1) the phase transformation in the solid state and dependence of the yield point on the temperature and the phase composition are taken into account. In the second model (example 2) the dependence of the yield point on the phase composition is not taken into consideration. In the third example the phase transformation in solid state is not included and the yield point is dependent on the temperature. Results of numerical calculations show differences between assumed models of welding.

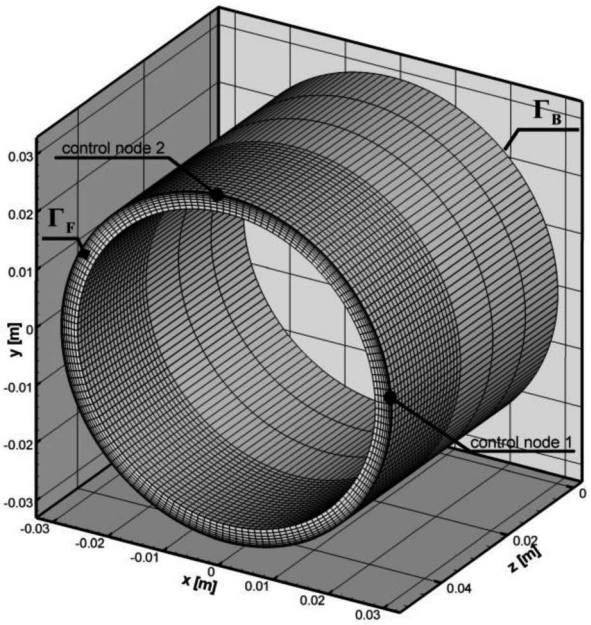

Fig. 6. Geometry of the welding element and mesh for Finite Element Method used in calculations. Control nodes are marked with black dot

Following boundary and initial conditions were introduced for the heat transport equation:

- Newton boundary condition on external and internal boundaries of the pipe with

  T_∞ =20°C, and α_{air} [W/m^{2}K] as follow

$$\alpha_{air} = \begin{cases} 0.0668 \times T & T_0 < T < 500\ ^\circ C \\ 0.231 \times T - 82.1 & T \geqslant 500\ ^\circ C \end{cases} \quad (21)$$

- Neumann boundary condition on the front boundaries Γ_F with q =0 W/m^2,
- Dirichlet boundary condition on back boundary Γ_B with T_D =20°C, the continuous of pipe is assumed,
- the initial temperature of the steel element T_0 =20°C,
- the parameters of the heat source: the welding speed v =0.0075 m/s, radius of the superficial source R=0.002 m, radius of the internal source R=0.0016 m, the power of superficial source F=700 W, the power of internal source Q=1470 W.

Following boundary and initial conditions completed stress model:

- Dirichlet boundary condition on boundaries Γ_B, with displacement $u_x = u_y = u_z = 0$,
- Dirichlet boundary condition on boundaries Γ_F, with displacement $u_z = 0$.

The CCT diagram of medium carbon steel for austenitization temperature was determined for 1200 [K] and was used in calculations [19]. Material properties used in calculations are collected in Tables 1-2 and Fig. 7.

TABLE 1
The material properties of steel element for numerical model

Material property	20°C	100°C	200°C	300°C	400°C	500°C	600°C	>600°C
λ[W/mK]	48.1	48.1	46.5	44	41	38.5	36.0	36.0
C[J/kgK]	481	502	519	531	569	670	712	712
ρ[kg/m^3]	7760							
L[J/kgK]	270000							
ν	0.3							
E_t [MPa]	$0.01 \times E$							
α_S	1.2×10^{-5}							

TABLE 2
The thermal and structural strain coefficients [7]

Phase	α_i [1/K]	γ_i
Austenite	2.178×10^{-5}	1.986×10^{-3}
Ferrite	1.534×10^{-5}	1.534×10^{-3}
Pearlite	1.534×10^{-5}	1.534×10^{-3}
Bainite	1.171×10^{-5}	4.0×10^{-3}
Martensite	1.36×10^{-5}	6.5×10^{-3}

The melting of material occurred on the entire circumference of the pipe wall thickness. Distribution of the austenite fraction in the track of source after the heating process is shown in Fig. 9.

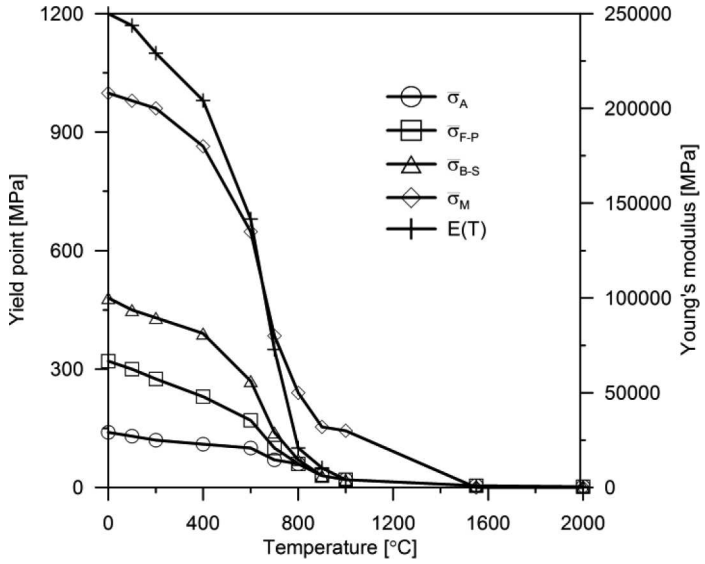

Fig. 7. The material properties of the steel element for the stress model

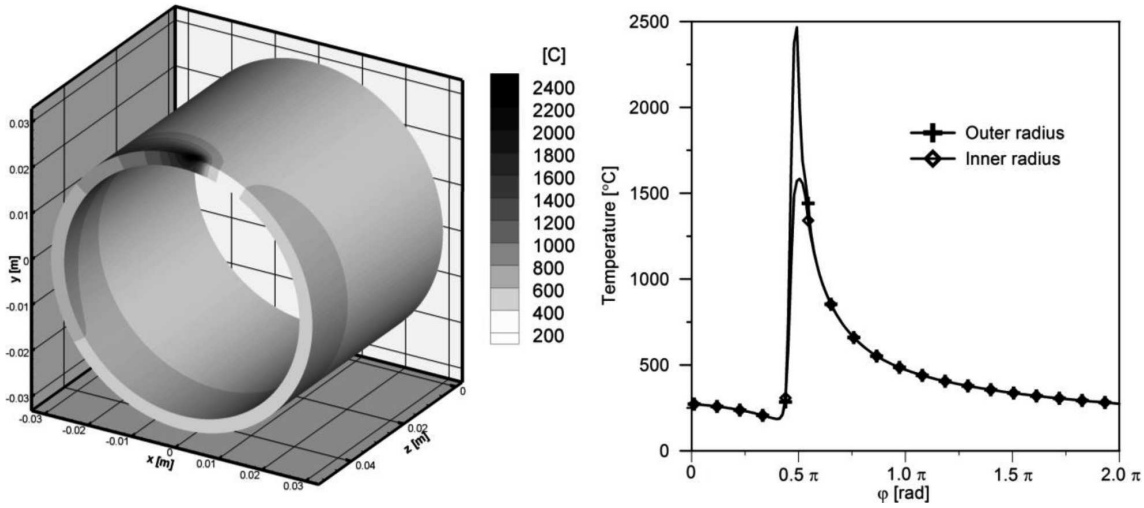

Fig. 8. Temperature for time of the process t= 25.6 s, a) field of temperature, b) distribution of temperature on the outer and inner radius on front boundary (Γ_F)

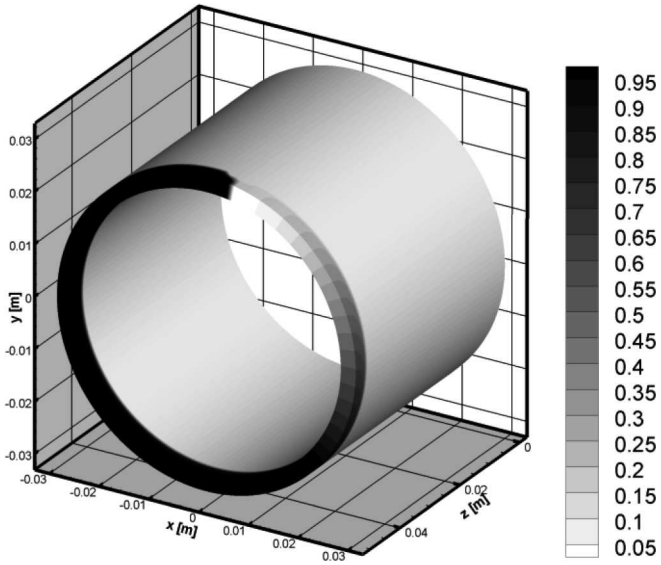

Fig. 9. Fraction of austenite for time of the process t= 25.6 s

The phase transformations in the control nodes according to time are presented in Figures 10-11. In the first control point one heating-cooling cycle is shown. High rate of cooling caused a formation of the martensitic phase. In the second control point two heating-cooling cycles and the transformation martensite to sorbite are visible.

In the Figures 12-14 the differences of values of effective stress between the analyzed numerical models are shown.

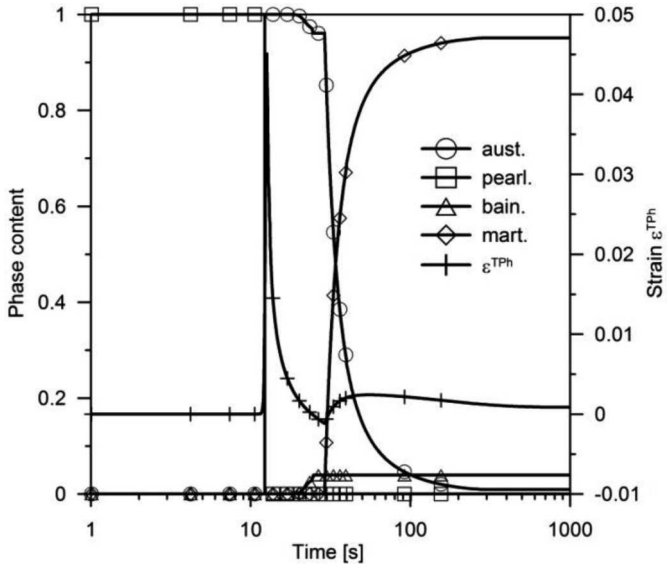

Fig. 10. Changes of participation of phases and strain in control node 1 according to time

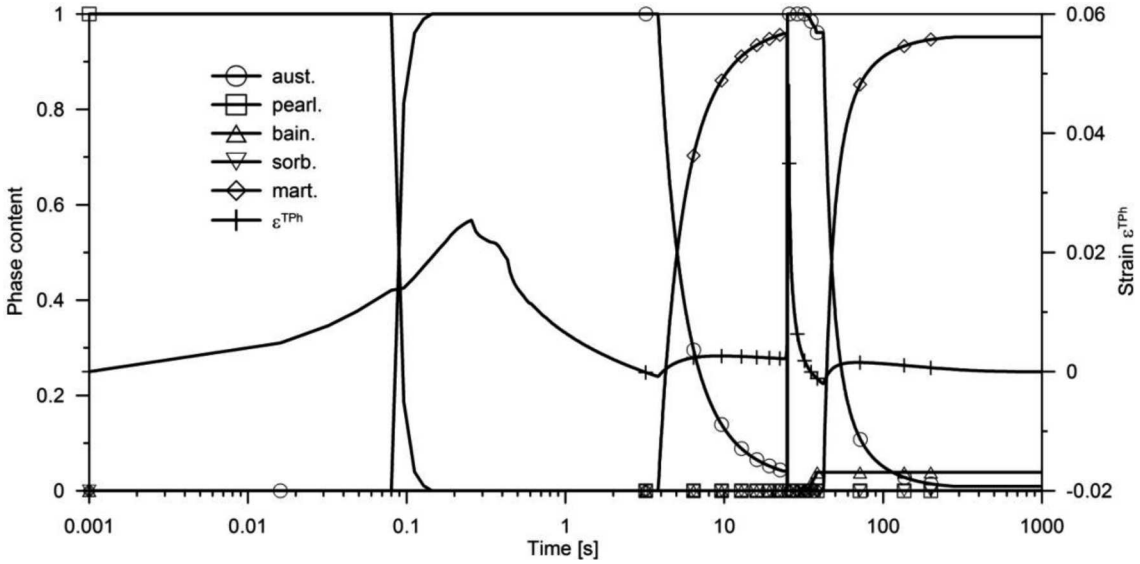

Fig. 11. Changes of participation of phases and strain in control node 2 according to time

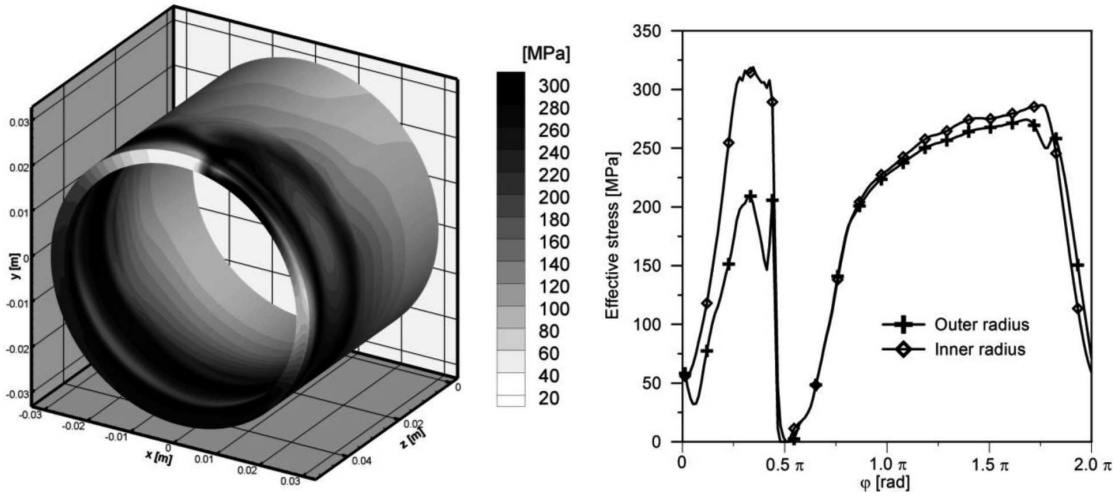

Fig. 12. The temporary effective stress for time of the process t= 25.6 s, the phase transformation in the solid state and dependence of the yield point on temperature is taken into account

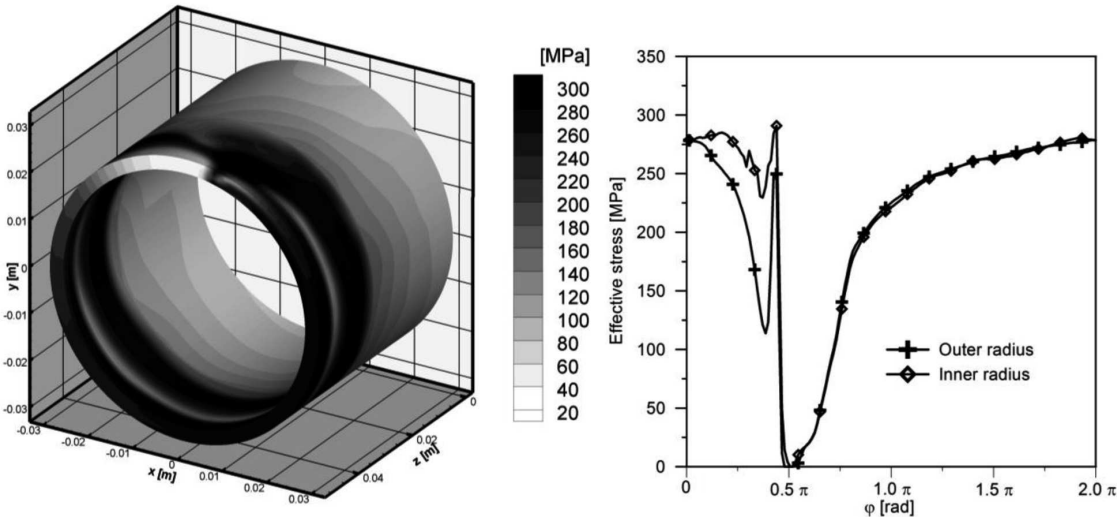

Fig. 13. The temporary effective stress for time of the process t= 25.6 s, dependence of the yield point on temperature is taken into account

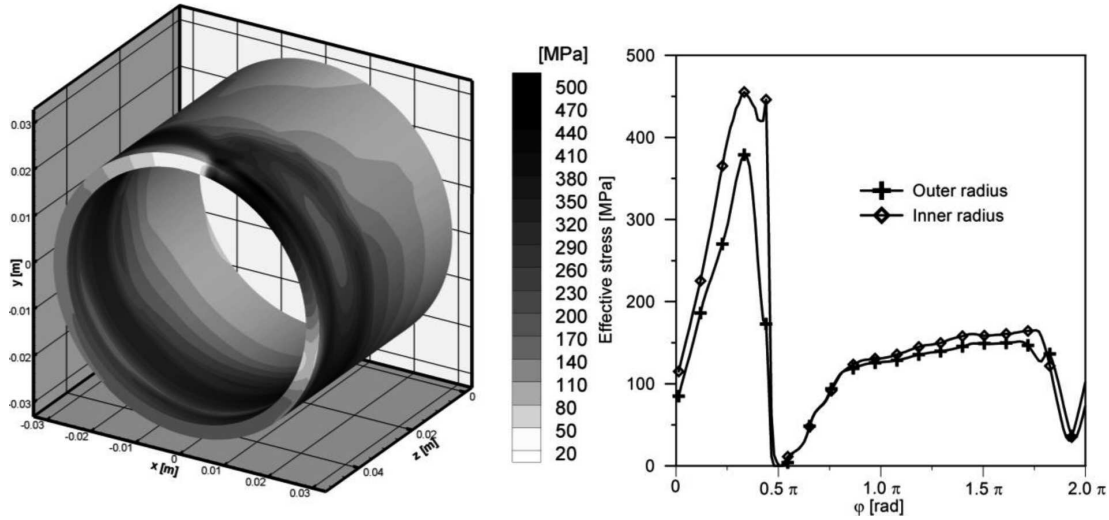

Fig. 14. The temporary effective stress for time of the process t= 25.6 s, the phase transformation in the solid state and dependence of the yield stress on temperature and phase transformation is taken into account

7. Conclusion

The following conclusions were obtained on the basis of numerical results:

- Models of laser welding must take into account a lot of feedback. In the considered cases some of them have a little importance. For example the latent heat of the transformation liquid-solid phase and the heat of transformation in the solid state have a little effect on the changes of temperature (high-speed of heating and cooling);
- In the model of welding process of medium carbon steel element the phase transformations in solid state should be contained. In particular, during cooling process the austenite-bainite and austenite-martensite transformation, and during heating process austenitization and martensite-sorbite transformation, should be taken into account;
- Depending of the material properties on the temperature is a necessary element in the model, in particular thermophysical properties for stress model;
- Depending of the yield point on the phase compositions of steel changes the distribution and values of temporary stresses significantly (Fig.12-14);
- Taking into account the structural strain in the welding model causes the change of the distribution of stress (Fig.12-14).

REFERENCES

[1] K.J. Lee, Characteristics of heat generation during transformation in carbon steels, Scripta Materialia **40**, 735-742 (1999).

[2] J.L. Lee, J.K. Cheny, Y.T. Pan, K.C. Hsieh, Evaluation of transformation latent heat in C-Mn steels, ISIJ International **39**, 281-287 (1999).

[3] E.P. Silva, P.M.C.L. Pacheco, M.A. Savi, On the thermo-mechanical coupling in austenite-martensite phase transformation related to the quenching process, International Journal of Solids and Structures **41**, 1139-1155 (2004).

[4] A. Bokota, Modelling of solidification and cooling of two-component metal alloys. Fields of temperature, concentrations and stresses, Monograph nr 79, Czestochowa (2001) (in Polish).

[5] W. Piekarska, M. Kubiak, A. Bokota, Numerical simulation of thermal phenomena and phase transformations in laser-arc hybrid welded joints, Archives of Metallurgy and Materials **56**(2), 409-421 (2011).

[6] B. Mochnacki, A. Nowak, A. Pocica, Numerical model of superficial layer heat treatment using the TIG method, Polska metalurgia w latach 1998-2002, 2, Komitet Metalurgii PAN, WN "Akapit", Kraków, 229-235 (2002).

[7] A. Kulawik, Numerical analysis of thermal and mechanical phenomena during hardening processes of the 45 steel, PhD Thesis, Częstochowa (2005) (in Polish).

[8] A. Kulawik, A. Bokota, The analysis of mutual influence of selected phenomena of hardening process for the C45 steel, KomPlasTech **1**, 231-238 (2005) (in Polish).

[9] H.J.M. Geijselaers, Numerical simulation of stresses due to solid state transformations. The simulation of laser hardening, Thesis University of Twente, The Netherlands (2003).

[10] J. Orlich, A. Rose, P. Wiest, Atlas zur Wärmebehandlung von Stähle, III Zeit Temperatur Austenitisierung Schaubilder, Verlag Stahleisen MBH, Düsseldorf, (1973).

[11] D.P. Koistinen, R.E. Marburger, A general equation prescribing the extent of the autenite-martensite transformation in pure iron-carbon alloys and plain carbon steels, Acta Metallica **7**, 59-60 (1959).

[12] M. Avrami, Kinetics of phase change, Journal of Chemical Physics **7**, 1103-1112 (1939).

[13] A. Bokota, A. Kulawik, Model and numerical analysis of hardening process phenomena for medium-carbon steel, Archives of Metallurgy and Materials Issue **2**, 52, 337-346 (2007).

[14] B. Chen, X.H. Peng, S.N. Nong, X.C. Liang, An incremental constitutive relationship incorporating phase transformation with the application to stress analysis, Journal of Materials Processing Technology **122**, 208-212 (2002).

[15] J. Winczek, A. Kulawik, Dilatometric and Hardness Analysis of C45 Steel Tempering with Different Heating-Up Rates, Metalurgija (Zagreb) **51** (1), 9-12 (2012).

[16] M. Kleiber, Finite element method in nonlinear continuum mechanics, Warszawa-Poznań, (1985), (in Polish).

[17] M. Coret, A. Combescure, A mesomodel for the numerical simulation of the multiphasic behavior of materials under anisothermal loading (application to two low-carbon steels), International Journal of Mechanical Sciences **44**, 1947-1963 (2002).

[18] L. Taleb, N. Cavallo, F. Waeckel, Experimental analysis of transformation plasticity, International Journal of Plasticity **17**, 1-20 (2001).

[19] F. Wever, A. Rose, Atlas zur Wärmebehandlung von Stähle, I Zeit Temperatur Umwandlungs Schaubilder, Verlag Stahl Eisen MBH, Düsseldorf, (1961).

Received: 10 May 2012.